Available online at www.sciencedirect.com
SCIENCE DIRECT
Journal of Catalysis 230 (2005) 464–475
JOURNAL OF CATALYSIS
www.elsevier.com/locate/jcat

Steam reforming of methanol over $Cu/ZrO_2/CeO_2$ catalysts: a kinetic study

A. Mastalir [a,b], B. Frank [b], A. Szizybalski [a], H. Soerijanto [a,b], A. Deshpande [c], M. Niederberger [c], R. Schomäcker [b], R. Schlögl [a], T. Ressler [a,*]

[a] *Fritz-Haber-Institut der MPG, Abteilung Anorganische Chemie, Faradayweg 4-6, 14195 Berlin, Germany*
[b] *Institut für Chemie, TU Berlin, Sekr. TC-8, Straße des 17. Juni 124, 10623 Berlin, Germany*
[c] *Max-Planck-Institut für Kolloid- und Grenzflächenforschung, Abteilung Kolloidchemie, MPI-KG 14424 Potsdam, Germany*

Received 19 October 2004; revised 16 December 2004; accepted 17 December 2004

Abstract

Steam reforming of methanol (SRM) was investigated over $Cu/ZrO_2/CeO_2$ (CZC) catalysts prepared via a novel synthetic method based on coprecipitation and polymer templating. Structural characterization of the samples was performed by N_2 adsorption–desorption, N_2O decomposition, and X-ray diffraction. The variation of the Cu loading resulted in an increased Cu crystallite size and a decreased specific surface area of the active particles. Catalytic investigations were carried out in a fixed-bed reactor at 10^5 Pa, with a $CH_3OH:H_2O$ ratio of 1:1. The samples with Cu contents higher than 5% exhibited good long-term stabilities and low CO levels during continuous operation. The kinetic model suggested for the transformation involved the reverse water–gas shift (RWGS) and methanol decomposition (MD), in addition to the SRM reaction. Kinetic measurements were made in the temperature range of 503–573 K, and the experimental results could be well simulated. The highest methanol conversions and the lowest CO levels were observed in the temperature range of 523–543 K. The apparent activation energies for the individual reactions were found to depend on the Cu content of the catalyst. Since the influence of mass transport limitations on the kinetic data could be excluded, it was established that the variation of the Cu concentration in the precursor material altered the microstructure of the Cu particles and, accordingly, the active Cu surface, which resulted in the formation of significantly different catalysts.

Keywords: Steam reforming of methanol; Copper; Zirconia; Ceria; N_2O chemisorption; Long-term stability; CO formation; Kinetic model; Reverse water–gas shift reaction; Methanol decomposition; Activation energy

1. Introduction

In the past decade, considerable attention has been focused on the reduction of the significant emissions originating from mobile sources, such as internal combustion engines [1–4]. For environmental reasons, the development of proton-exchange membrane fuel cells (PEMFCs) has gained in importance [5,6]. As compared with conventional heat engines, several advantages of fuel cell application have been established, including a higher efficiency and a more convenient operation, the absence of moving parts, and the low emission of hazardous compounds [1,5]. The combustion of hydrogen in a fuel cell is regarded as a clean process, releasing energy and providing only water as an exhaust material [4,7,8]. However, hydrogen is not a natural energy source; its generation consumes a large amount of energy, either from natural gas or via the electrolysis of water [4]. Furthermore, for a fuel-cell vehicle, the storage and the supply of hydrogen, a volatile and explosive gas, impose mechanical problems and safety hazards on a commercial level [1,4,8].

Several liquid fuel candidates have been discussed for on-board reforming, including methanol, ethanol, gasoline, and diesel [1], of which methanol is considered the most

* Corresponding author. Fax: +49 30 8413 4405.
E-mail address: ressler@fhi-berlin.mpg.de (T. Ressler).

0021-9517/$ – see front matter © 2005 Published by Elsevier Inc.
doi:10.1016/j.jcat.2004.12.020

favorable alternative [1,9]. Although mostly produced from natural gas, methanol can also be obtained from renewable sources, thus lowering the amount of carbon dioxide produced [5,9]. Moreover, via methanol synthesis from hydrogen and carbon dioxide, methanol can be employed as a storage and transport medium for hydrogen. In addition to its good availability and low boiling point, methanol possesses a high hydrogen/carbon ratio (4/1) and contains no carbon–carbon bond, which considerably reduces the risk of coke formation during its reactions [1,5,6].

The most important processes for the production of hydrogen from methanol:

$$\mathrm{CH_3OH(g)} \underset{k_{-\mathrm{D}}}{\overset{k_{\mathrm{D}}}{\rightleftharpoons}} 2\mathrm{H_2} + \mathrm{CO}, \quad \Delta H^\circ = 91\ \mathrm{kJ\,mol^{-1}}; \tag{1}$$

$$\mathrm{CH_3OH(g)} + \mathrm{H_2O(g)} \underset{k_{-\mathrm{R}}}{\overset{k_{\mathrm{R}}}{\rightleftharpoons}} \mathrm{CO_2} + 3\mathrm{H_2}, \quad \Delta H^\circ = 50\ \mathrm{kJ\,mol^{-1}}; \tag{2}$$

$$\mathrm{CH_3OH(g)} + 0.5\mathrm{O_2} \underset{k_{-\mathrm{O}}}{\overset{k_{\mathrm{O}}}{\rightleftharpoons}} 2\mathrm{H_2} + \mathrm{CO_2}, \quad \Delta H^\circ = -192\ \mathrm{kJ\,mol^{-1}} \tag{3}$$

are decomposition (MD), steam reforming (SRM), and partial oxidation (POM) [1]. The combined or oxidative reforming of methanol (CRM or OSRM), a combination of (2) and (3), has also been investigated [2,6,10,11]. The decomposition of methanol is a strongly endothermic reaction producing a high CO yield, which makes it rather unsuitable for fuel-cell applications [1]. The steam reforming reaction is also endothermic; however, it typically affords a substantial H_2 yield of 75%, while maintaining high carbon dioxide selectivity ($\sim$ 25%) [1,4,8]. The partial oxidation of methanol is an exothermic reaction with a rapid start-up and a dynamic response [4]. Nevertheless, the formation of hot spots in the reactor may result in sintering of the Cu particles, which tends to decrease the catalytic performance [8,11]. Furthermore, this reaction produces a considerably lower amount of hydrogen than SRM [1,8,9].

As the highest hydrogen yield may be achieved by the steam reforming of methanol [1], the latter reaction was investigated within the framework of the present study. The major drawback of SRM is the formation of CO as a by-product, which, even at a low concentration of 100 ppm, decreases the fuel-cell performance by poisoning the Pt electrode [2,6,12]. Currently, second-stage catalytic reactors are being used to remove CO by the water–gas shift reaction, oxidation, or methane formation [6,10]. However, this CO clean-up unit is rather inconvenient, as it occupies a large volume and decreases the efficiency of the fuel cell through hydrogen consumption [8]. To eliminate the need for gas purification, high-performance catalysts are required that provide substantial methanol conversion and H_2 selectivity, together with the lowest possible amount of CO [10,12]. The complete absence of CO in the product gas may be difficult to achieve under SRM conditions.

Several studies have been reported in the literature on the applications of Cu- and Pd-based catalysts for SRM [1–6,8–18], of which Cu-containing catalysts are clearly preferred because of their high activity and selectivity at lower temperatures [1,12,19]. Although Cu catalysts are also regarded as susceptible to thermal deactivation, their sintering abilities may be considerably reduced by the addition of one or more oxide species, such as ZnO, Al_2O_3, or Cr_2O_3 [20]. The most efficient catalysts for SRM, including the traditional Cu/ZnO and Cu/ZnO/Al_2O_3 systems, have been investigated in detail [1,3,6,9,15,16,21–25]. The in situ characterization of Cu/ZnO under SRM activation and operating conditions revealed that the interaction of the Cu and ZnO phases has a pronounced effect on the catalytic activity [22,23]. For Cu/ZnO/Al_2O_3 catalysts, high methanol conversions and low CO selectivities have been obtained [1,5,8,9,16] and kinetic analysis has provided important information on the overall reaction mechanism [5,6,16,21,25,26]. Compared with the conventional ZnO- or Al_2O_3-supported Cu catalysts, ZrO_2-containing samples have shown increased activities and reduced CO levels for the SRM reaction [3,5,12,27–29]. The promoting effect of ZrO_2 has been attributed to an improved reducibility of CuO, which tends to increase the Cu dispersion [29]. ZrO_2 has also been reported to prevent the sintering of Cu crystallites under reaction conditions [5,12,29] and thus may be regarded as a structural stabilizer. Likewise, the application of CeO_2, as either a support material or a promoter, has been found to improve the efficiency of Cu-based catalysts [11,30,31]. CeO_2 has been found to increase the thermal stability and the activity of Al_2O_3-supported Cu catalysts through a synergetic effect and to favor the conversion of CO via the water–gas shift reaction [30]. Moreover, CeO_2 has a high oxygen storage capacity [32,33], and the partially reduced CeO_2 sites formed under reductive conditions produce mobile oxygen, which tends to have a beneficial effect on the catalytic performance [31,32]. For ZrO_2–CeO_2-supported catalysts, the interaction between the oxide phases, leading to the formation of a thermally stable solid solution, has been reported to increase the mobility of oxygen in both phases [32].

The aim of the current work was the structural and catalytic investigation of novel Cu/ZrO_2/CeO_2 catalysts prepared by coprecipitation. To increase the specific surface area, highly porous polymer beads were employed as a template for the preparation of the solid catalysts [34]. Samples with different Cu loadings were examined for the steam reforming of methanol; their catalytic properties, including long-term stability and CO production, are discussed here. Furthermore, the reaction mechanism was studied and a kinetic analysis was undertaken to determine the rate constants and the activation energies for the model reactions.

2. Experimental

2.1. Catalyst preparation

The $Cu/ZrO_2/CeO_2$ (CZC) catalysts were synthesized from metal sols, prepared from the appropriate amounts of the mixed precursors $(NH_4)_2Ce(NO_3)_6$, $ZrO(NO_3)_2 \cdot H_2O$, and $Cu(NO_3)_2 \cdot 2.5H_2O$ (all Aldrich products of $> 99\%$ purity) dissolved in 40 ml of distilled water. The total metal content of the resulting sol was 5×10^{-3} mol. We coprecipitated the metal sols as metal hydroxides by increasing the pH above 10 through the addition of a NaOH solution. The resulting precipitate was repeatedly washed with distilled water until a pH of 7 was obtained, and then suspended in a mixture of 5 ml of distilled water and a calculated amount of 90% HNO_3. Depending on the sample composition, the HNO_3/metal molar ratio was varied between 1/1 and 1.5/1. Ultrasonic treatment of the suspension for 45–60 min resulted in the formation of a transparent sol [35].

Templating was carried out with XAD-16 nonfunctionalized polystyrene beads (a Sigma product), with a specific surface area of 800 $m^2\,g^{-1}$ and an average pore diameter of 10 nm. The wet beads (1.5 ml) and the metal sol (0.005 mol) were mixed together and then heated in an oven at 333 K for 2 days to ensure solvent evaporation. The beads were subsequently dried at 373 K for another day and then washed with distilled water to remove any excess deposit from their surface. After drying at 333 K for 1 day, the samples were calcined in an oven at 773 K in a N_2 stream of 100 ml/min for 2.5 h and then for an additional 8 h in air. Upon calcination gray–green materials were obtained (see Fig. 1). Because of the mean particle diameter (500 μm) and the regular character of the polymer beads, the resulting CZC samples could be conveniently applied as catalysts in fixed-bed reactors.

Four representative CZC samples were synthesized by the above method, with Cu contents of 5, 15, 25, and 35% (denoted CZC5, CZC15, CZC25 and CZC35, respectively), to be characterized and tested for the steam reforming of methanol. A ZrO_2/CeO_2 molar ratio of 1/1 for the support materials was maintained in each case.

2.2. Characterization

2.2.1. X-ray fluorescence analysis

The results of the elementary analysis of the CZC samples, performed with a Seiko (SEA 2010) instrument, are shown in Table 1. The amount of Cu detected in the samples was found to be only slightly lower than that expected from the preparation conditions, and the ratio $ZrO_2/CeO_2 = 1/1$ proved to be well adjusted.

2.2.2. N_2 adsorption–desorption

The specific surface areas of the CZC samples were determined from N_2 adsorption–desorption data obtained at the temperature of liquid N_2 (77 K), by using a Micromeritics 2375 BET apparatus equipped with a Vacprep 061 degasser. To remove traces of water and impurities from the surface, all samples were degassed before measurement at 13 Pa and 393 K for 12 h. The specific surface areas were calculated from the BET equation, and the average pore diameters (d_p) were obtained by the BJH method from the desorption branches of the adsorption isotherms.

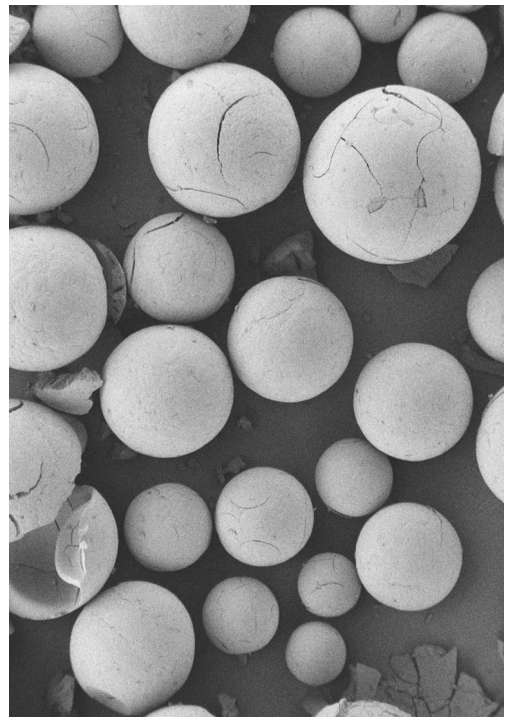

Fig. 1. Scanning electron micrograph of a $Cu/ZrO_2/CeO_2$ catalyst (CZC5) after calcination.

Table 1
Characteristic data of the CZC catalysts

Sample	Cu (%)	Zr (%)	Ce (%)	BET area ($m^2\,g^{-1}$)	d_p (nm)	Cu^0 area ($m^2\,g_{cat}^{-1}$)	Cu^0 area ($m^2\,g_{Cu}^{-1}$)
CZC5	4.4	44.6	51.0	96	9.4	0.9	51.4
CZC15	12.1	44.3	43.6	102	9.9	1.8	25.8
CZC25	23.9	37.6	38.5	94	9.8	1.8	12.2
CZC35	31.0	32.7	36.3	83	10.0	1.5	7.6

2.2.3. N_2O decomposition

The specific Cu^0 surface areas of the samples were measured by N_2O decomposition, with the reactive frontal chromatography (RFC) method introduced by Chinchen et al. [36].

The method is based on the oxidation of the exposed Cu^0 surface atoms of a reduced sample when the feed is switched from an inert gas stream to a mixture containing N_2O as an oxidizing species. The Cu^0 surface area can then be determined from the amount of N_2O consumed in the reaction

$$2Cu + N_2O \rightarrow Cu_2O + N_2. \quad (4)$$

Before measurements, the CZC samples were activated in a stream of $MeOH/H_2O$ (2/1) with a flow rate of 36 $cm^3\,min^{-1}$ at 523 K. To diminish the amount of adsorbed molecules on the Cu surface, the samples were subsequently purged in pure He (50 $cm^3\,min^{-1}$) at 523 K for 1 h and then cooled to 313 K, where the measurements were performed in a 0.5% N_2O/He stream of 15 $cm^3 min^{-1}$. The catalysts were diluted with boron nitride to provide a sample bed with a height of ca. 25 mm, with a thermocouple positioned directly inside the powder bed. The material was placed on a quartz frit in a tubular quartz reactor.

For the RFC method described by Chinchen et al., the area under the ion current trace ($m/e = 28$ for N_2) has been used directly to determine the Cu^0 surface area. For the current experiments, however, the same MS signal obtained from the amount of N_2 produced for the CZC samples was found to be insufficient for evaluation. Therefore, the amount of N_2 formed during decomposition was indirectly estimated from the retarded evolution of N_2O ($m/e = 44$), as compared with blank experiments performed with boron nitride. Earlier investigations for Cu/ZnO samples revealed a good agreement between the Cu^0 surface areas determined by N_2O RFC and those obtained from the Cu crystallite size [23,37]. We calculated the Cu^0 surface area, assuming a stoichiometry of $N_2O/Cu = 0.5$ and a value of 1.47×10^{19} Cu atoms/m^2 for the surface density [5,29,36].

2.2.4. X-ray diffraction

Ex situ X-ray diffraction (XRD) measurements were performed with a STOE STADI P transmission diffractometer (Cu-K_α radiation, Ge monochromator) equipped with a position-sensitive detector (PSD) (internal resolution $2\Theta = 0.01°$). The CuO crystallite diameters were calculated from the Scherrer equation [38]. The full width at half-maximum (FWHM) was determined by fitting a Lorentzian profile function to the CuO (111) and (200) diffraction peaks at $2\Theta = 38.371°$ and 38.923°, respectively.

2.3. Catalytic test reaction

The steam reforming of methanol was studied in a fixed-bed tubular reactor (stainless steel, i.d. = 10 mm) with the use of a three-channel set-up, which ensured that three catalysts could be investigated at the same time, under exactly the same conditions. To achieve an efficient heat transfer, the reactors were placed in an aluminum heating block. The temperature of the reactor was regulated by PID control of the cartridge heaters situated inside the aluminum block. Time-on-stream investigations were performed at 523 K, and the mass of catalyst was varied between 0.100 and 0.770 g, depending on the Cu content, to keep the amount of CuO constant for all samples (0.0225 g). For kinetic measurements, the mass of catalyst was increased by a factor of 2.6, corresponding to a CuO content of 0.0584 g for each sample, to achieve full conversion in the temperature range investigated (503–573 K). The catalyst was supported inside the reactor by a stainless-steel grid. For flow conditioning, inert Pyrex beads ($d = 500$ μm) were placed below and on top of the catalyst bed. The reactant mixture of MeOH (HPLC grade, 99.9% purity) and distilled water, with a $MeOH/H_2O$ molar ratio of 1/1, was introduced into the reactor with a Dionex HPLC P 580 pump. Both reactants were degassed before use at 20 kPa. For time-on-stream measurements, the flow rate for a single channel was 0.07 $cm^3\,min^{-1}$, whereas for kinetic investigations, it was varied between 3.33×10^{-3} and 0.67 $cm^3\,min^{-1}$. Kinetic measurements were made with fresh catalysts to eliminate aging effects, and experimental data were collected after 5 days on stream. To achieve steady-state conditions, experimental data at low flow rates were collected 60 min after the flow rate had been adjusted. Before measurement, the catalysts were activated in situ in a $MeOH/H_2O = 1/1$ stream of 0.07 $cm^3\,min^{-1}$ at 523 K for 16 h [15,16,25].

The reaction products, consisting of effluent gases (H_2 and CO_2 as main products and a minor amount of CO), together with unreacted methanol and water, were passed through a condenser at 268 K, which removed most of the liquid from the product gas stream. Complete removal of the condensed reactant mixture was achieved with an additional condenser at 253 K. The liquid composition was analyzed with an Intersmat gas chromatograph (GC), equipped with a thermal conductivity detector (TCD), operated with a 50 m × 0.53 mm CP-Wax column at 363 K. The composition of the dry product gas mixture was determined on-line, with a Varian 3800 GC with a TCD. Helium was applied as a carrier gas, and separation was achieved with a 25 m × 0.53 mm CarboPLOT P7 column at 304 K. For quantitative analysis of the product gas stream, a calibration gas mixture, containing 0.5% CO, 4.5% N_2, 25% CO_2, and 70% H_2 (a Messer Griesheim product), was used. Under the present experimental conditions, no evidence for the formation of the by-products methane, methyl formate, or dimethyl ether was found [27,39].

3. Results and discussion

3.1. Catalyst characterization and long-term stability

The results obtained for the CZC samples from N_2 adsorption–desorption and N_2O decomposition are summarized in Table 1.

The BET surface areas obtained for the CZC samples were higher than those reported for ZnO-supported Cu catalysts [39] and of an order similar to those published for Cu/Al_2O_3 samples by Cheng et al. [19]. A decreasing BET surface area with increasing Cu loading [19] was observed only for the samples with Cu contents exceeding 5%. As seen in Table 1, the values for the average pore diameter were very close for each sample (9.35–10.0 nm). Although the Cu^0-specific surface areas for the CZC materials proved to be lower than expected from the internal surface areas and

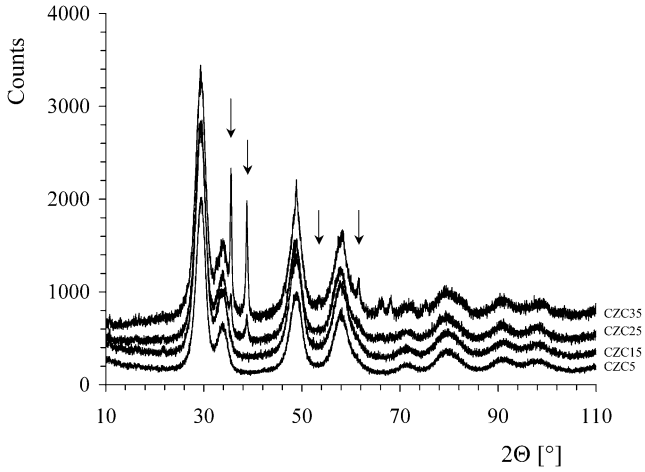

Fig. 2. X-ray diffraction patterns of four CZC catalysts with a nominal copper concentration of 5% (CZC5), 15% (CZC15), 25% (CZC25), and 35% (CZC35) with a constant ZrO_2/CeO_2 ratio of about 1. Arrows indicate CuO phase.

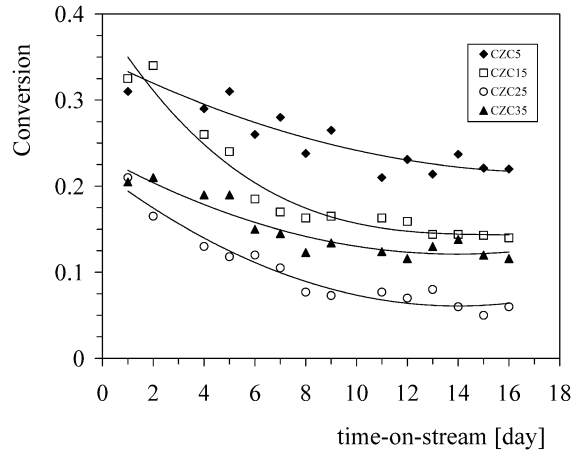

Fig. 3. Methanol conversions during SRM of four CZC catalysts as a function of time-on-stream ($m_{CuO} = 0.0225$ g, $T = 523$ K, $p = 10^5$ Pa, $w = 0.07$ cm^3 min^{-1}, $MeOH/H_2O = 1/1$).

the Cu contents [29], the values exhibited a trend similar to that of the BET results. The highest Cu^0 surface area per gram of copper was obtained for CZC5. An increasing Cu content resulted in a decreasing Cu^0 surface area roughly in agreement with an increasing Cu particle size. The net decrease in the Cu^0 specific surface area with increasing Cu content, observed for CZC15, CZC25, and CZC35, is in correlation with earlier results reported in the literature for supported Cu catalysts [5,19].

The XRD patterns of the CZC samples displayed in Fig. 2 revealed that the characteristic CuO peaks could be distinguished only for the samples with the highest Cu contents. The absence of CuO signals for CZC5 and CZC15 may be attributed in part to their lower Cu loading. Furthermore, the Cu crystallite size for the above samples may be too small to be detected by XRD, as related to a pronounced line broadening [5]. The broadening of the peaks also renders it difficult to establish whether the Zr, Ce, and O atoms are arranged in a single mixed phase or in separate phases. For the same reason, the corresponding crystal structures (cubic and/or tetragonal) cannot be reliably determined. The Cu crystallite sizes obtained from the diffraction peaks for CZC25 and CZC35 were 12.4 and 15.3 nm, respectively. The slight increase in the particle size observed for the latter sample is in line with the decrease in the Cu^0-specific surface area obtained from N_2O decomposition. Further structural data on the $Cu/CeO_2/ZrO_2$ catalysts obtained under reaction conditions and corresponding structure-activity relationships will be presented elsewhere.

To make a comparison between the long-term stabilities of the CZC catalysts, the methanol conversions obtained during a continuous operation of 16 days under standard conditions were plotted as a function of time on stream (Fig. 3).

It can be seen that no linear correlation exists between the catalytic activity depicted in Fig. 3 and the Cu surface area (Table 1). Evidently, the catalytic activity of the CZC samples is determined not only by the Cu surface area, but also by the particular microstructure of the Cu particles, which may be similar to the microstrain in Cu/ZnO catalysts [23]. The catalytic activities of all of the samples were found to diminish considerably for a period of 5 days, although to a different extent, which displayed no systematic variation with the Cu content. The conversions determined after 5 days approached a constant value, except for that of CZC5, which exhibited a further decrease. After an initial period of deactivation, the CZC samples with Cu contents exceeding 5% displayed good long-term stabilities, and, hence, these samples may be suitable for extended operation. The relatively poor thermal stability of CZC5 may be related to the small Cu particle size, in light of the fact that small particles tend to be more susceptible to thermal sintering under reaction conditions [40], even at temperatures lower than 523 K [41]. In addition to the CZC samples, a copper-free CeO_2/ZrO_2 sample was prepared with the same procedure as described above. This material did not exhibit any detectable activity in the steam reforming of methanol under the reaction conditions employed. Hence, the differences observed for the CZC catalysts in the steam reforming of methanol can be attributed mainly to the bulk and surface properties of the Cu phase in these materials.

The CO partial pressures determined during the above measurements are depicted in Fig. 4. As mentioned above, the sample masses were adjusted to provide the same Cu content. For this reason, the mass of CZC5 considerably exceeded those of the other samples, and this may account for the substantially higher amount of CO detected for CZC5 than for the samples with higher Cu contents. Moreover, following a pronounced decrease for about 5 days, the CO levels were stabilized and did not exhibit any significant difference. This finding is consistent with the results of N_2O decomposition, indicating that the active Cu contents of these samples were very similar. It may be concluded from Figs. 3 and 4 that an increase in the Cu content from 5 to 15% has a beneficial effect on the catalytic performance of

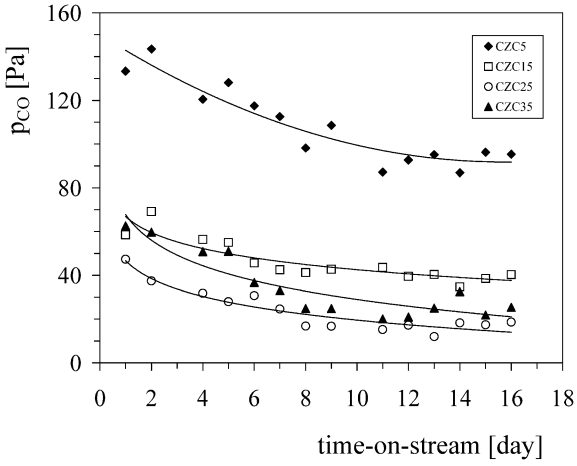

Fig. 4. CO formation during SRM of four CZC catalysts as a function of time-on-stream ($m_{CuO} = 0.0225$ g, $T = 523$ K, $p = 10^5$ Pa, $w = 0.07$ cm^3 min^{-1}, MeOH/$H_2O = 1/1$).

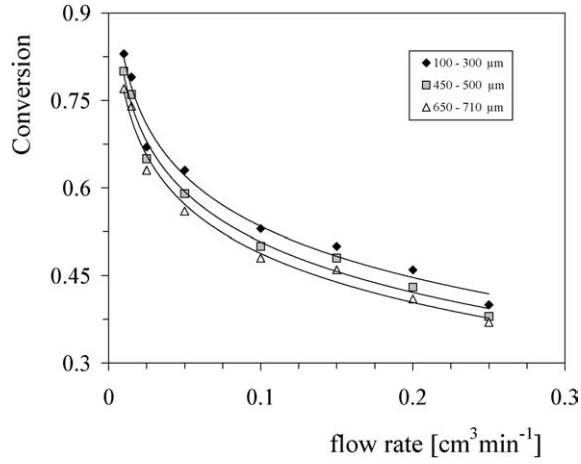

Fig. 5. Methanol conversions during SRM as a function of the reactant flow rate, determined for various sieve fractions of CZC15 ($m = 0.5500$ g, $T = 523$ K, $p = 10^5$ Pa, MeOH/$H_2O = 1/1$).

CZC through improvement of the long-term stability and suppression of the CO production. Although the effect of a further increase in the Cu loading proved to be less important for the stability of the catalyst, it resulted in lower CO levels. Nevertheless, the CO production is also dependent on the conversion of methanol [29], as the activity order of the CZC samples (Fig. 3) is in correlation with the order of the CO levels throughout the entire time-on-stream interval (Fig. 4). Accordingly, under the present experimental conditions, the samples with increased Cu contents may be regarded as more efficient catalysts for SRM, with respect to the formation of CO in particular.

Inasmuch as the CZC catalysts are porous materials and the methanol conversions in Fig. 3 displayed no systematic variation with either the Cu loading or the Cu^0 surface area, the effect of mass transport limitations on the catalytic performance was also investigated. It was previously observed that the CZC samples were not uniform in size. Thus, for each material, three fractions with different particle diameters could be obtained by sieving. Moreover, a Cu/CeO_2 sample containing 25% Cu, prepared by the same method, was found to deteriorate slightly during SRM, as a small amount of the original catalyst beads (3.3%) were transformed into a fine powder after reaction. On the other hand, the Zr-containing beads of the CZC samples remained essentially unchanged after catalytic investigations, which confirms that ZrO_2 is an important structural stabilizer [12,29]. The methanol conversions obtained for the different sieve fractions of CZC15 under the same conditions are plotted in Fig. 5 as a function of the reactant flow rate.

When the flow rate was increased, the conversions for the various sieve fractions declined to the same extent. At a given flow rate, the values obtained decreased slightly with an increasing particle diameter; however, the differences detected were not significant with respect to mass transport limitation. This is corroborated by the dependence of the CO

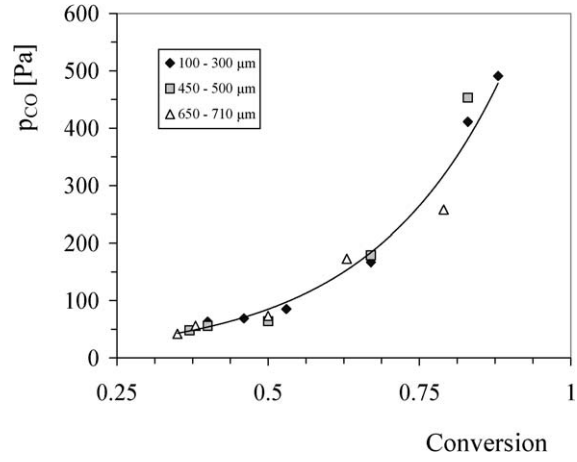

Fig. 6. CO partial pressures determined for various sieve fractions of CZC15 during SRM under standard conditions ($m = 0.5500$ g, $T = 523$ K, $p = 10^5$ Pa, MeOH/$H_2O = 1/1$).

partial pressure on the methanol conversion, as depicted in Fig. 6.

According to Fig. 6, the CO levels for the three fractions at the same conversions were very similar, and thus all values could be fitted with the same exponential function. It may therefore be concluded that intraparticle transport phenomena exerted no considerable influence on the CO formation. Hence, because mass transport limitations can be excluded, a reliable kinetic model was suggested for the steam reforming of methanol. We determined the kinetic parameters by fitting the model to the experimental results obtained for the CZC catalysts.

3.2. Kinetic model

The individual reactions to be included in the kinetic model of the methanol steam reforming process are still under debate. Earlier studies have suggested that the kinetics could be sufficiently described with the use of only one

or two of the possible overall reactions, under the assumption that the others were at equilibrium or their rates were negligible. Initially, SRM was supposed to proceed by the formation of CO and H_2, followed by the water–gas shift (WGS) reaction [15,42]. The formation of CO_2 by the direct reaction of methanol and steam has also been proposed [43]. Methanol decomposition was involved in the reaction mechanism in certain studies [14,42,44], whereas in other cases, it was regarded as insignificant [16,21].

An adequate kinetic model for the steam reforming of methanol on a commercial $Cu/ZnO/Al_2O_3$ catalyst, which includes methanol decomposition [Eq. (1)] and the WGS reaction [Eq. (5)], in addition to the SRM process [Eq. (2)], has recently been suggested by Peppley et al. [25]

$$\mathrm{CO} + \mathrm{H_2O(g)} \underset{k_{-\mathrm{W}}}{\overset{k_{\mathrm{W}}}{\rightleftharpoons}} \mathrm{CO_2} + \mathrm{H_2}, \quad \Delta H^\circ = -41\ \mathrm{kJ\,mol^{-1}}. \tag{5}$$

Further investigations of SRM revealed that the above model may also apply for other catalysts, including Zr- or Ce-containing systems [28–30]. For the present study, it was found that a kinetic evaluation that included MD in the reaction scheme afforded a better fit to the experimental data. Accordingly, evaluation of the experimental data obtained for the CZC samples was based on Peppley's model. The kinetic model suggested by Takahashi et al., involving a methyl formate intermediate [45], may be regarded as less suitable for evaluation, given that no methyl formate production was observed under the present experimental conditions. In fact, methyl formate is more likely to be formed when the reaction is conducted in an excess of methanol [3].

CO formation has generally been observed at high methanol conversions and long contact times, indicating that CO is a secondary product, formed by the reverse water–gas shift (RWGS) reaction [3,6,28]. For the CZC samples, kinetic analysis suggested that the amount of CO produced by MD was considerably lower than that formed by the RWGS reaction, and therefore we simplified the reaction scheme by regarding MD as an irreversible reaction. Furthermore, because of the low Hüttig temperature of Cu [46], as reflected in its relatively low melting point (1356 K) [5,6], Cu-based catalysts tend to undergo thermal deactivation at temperatures exceeding 573–623 K [5,6,47]. To eliminate aging effects, kinetic measurements for the CZC samples were carried out in the temperature range of 503–573 K.

According to the above considerations, the reaction scheme utilized for methanol steam reforming on CZC catalysts included the MD, SRM, and RWGS reactions [Eqs. (1), (2), and (5)]. Because SRM is the sum of the other two reactions, the above processes are not independent [26]. We calculated the partial pressures of the reactants and products with the assumption that the contribution of MD to the conversion was negligible. If the SRM reaction for an equimolar mixture of methanol and water takes place with a conversion of X, then the total mole number after SRM is $n = n_0(1 + X)$. If we assume that the RWGS reaction proceeds with a conversion of X_{w}, the partial pressures of the reactants and products can be expressed as follows:

$$p_{\mathrm{CO}} = \frac{X X_{\mathrm{w}}}{2 + 2X} p, \tag{6}$$

$$p_{\mathrm{CO_2}} = \frac{X(1 - X_{\mathrm{w}})}{2 + 2X} p, \tag{7}$$

$$p_{\mathrm{H_2}} = \frac{X(2 + X_{\mathrm{w}})}{2 + 2X} p, \tag{8}$$

$$p_{\mathrm{MeOH}} = \frac{1 - X}{2 + 2X} p, \tag{9}$$

$$p_{\mathrm{H_2O}} = \frac{1 - (1 - X_{\mathrm{w}})X}{2 + 2X} p. \tag{10}$$

The partial pressures can be obtained from Eqs. (6)–(10), given that $p = 10^5$ Pa, and X_{w} can be calculated from Raoult's law as

$$X_{\mathrm{w}} = \frac{\varphi_{\mathrm{CO}}}{\varphi_{\mathrm{CO}} + \varphi_{\mathrm{CO_2}}}, \tag{11}$$

where φ_{CO} and $\varphi_{\mathrm{CO_2}}$ are the volume fractions for CO and CO_2, respectively, which can be determined from the corresponding GC peak areas after the calibration gas mixture has been analyzed.

The rate equations for the model reactions [Eqs. (1), (2), and (5)] can be described as follows:

$$r_{\mathrm{SRM}} = k_{\mathrm{R}} p_{\mathrm{MeOH}}^{\mathrm{m_1}} p_{\mathrm{H_2O}}^{\mathrm{m_2}} - k_{-\mathrm{R}} p_{\mathrm{CO_2}}^{\mathrm{m_3}} p_{\mathrm{H_2}}^{3\mathrm{m_4}}, \tag{12}$$

$$r_{\mathrm{MD}} = k_{\mathrm{D}} p_{\mathrm{MeOH}}^{\mathrm{m_5}}, \tag{13}$$

$$r_{\mathrm{RWGS}} = k_{-\mathrm{W}} p_{\mathrm{CO_2}}^{\mathrm{m_6}} p_{\mathrm{H_2}}^{\mathrm{m_7}} - k_{\mathrm{W}} p_{\mathrm{CO}}^{\mathrm{m_8}} p_{\mathrm{H_2O}}^{\mathrm{m_9}}. \tag{14}$$

Accordingly, the differential equations for the single components (obtained with the Maple V software, release 4.00c) are given below:

$$\frac{\partial p_{\mathrm{MeOH}}}{\partial t} = -(r_{\mathrm{SRM}} + r_{\mathrm{MD}}) \frac{2}{1 + X}, \tag{15}$$

$$\frac{\partial p_{\mathrm{H_2O}}}{\partial t} = -(r_{\mathrm{SRM}} + r_{\mathrm{RWGS}}) - (r_{\mathrm{SRM}} + r_{\mathrm{MD}}) \frac{p_{\mathrm{H_2O}}}{p_{\mathrm{MeOH},0}}, \tag{16}$$

$$\frac{\partial p_{\mathrm{CO}}}{\partial t} = (r_{\mathrm{MD}} + r_{\mathrm{RWGS}}) - (r_{\mathrm{SRM}} + r_{\mathrm{MD}}) \frac{p_{\mathrm{CO}}}{p_{\mathrm{MeOH},0}}, \tag{17}$$

$$\frac{\partial p_{\mathrm{CO_2}}}{\partial t} = (r_{\mathrm{SRM}} - r_{\mathrm{RWGS}}) - (r_{\mathrm{SRM}} + r_{\mathrm{MD}}) \frac{p_{\mathrm{CO_2}}}{p_{\mathrm{MeOH},0}}, \tag{18}$$

$$\frac{\partial p_{\mathrm{H_2}}}{\partial t} = (3r_{\mathrm{SRM}} + 2r_{\mathrm{MD}} - r_{\mathrm{RWGS}}) - (r_{\mathrm{SRM}} + r_{\mathrm{MD}}) \frac{p_{\mathrm{H_2}}}{p_{\mathrm{MeOH},0}}. \tag{19}$$

The increased mole numbers during SRM (4 mol of products formed from 2 mol of reactants) were taken into account via expression of the conversion X by the partial pressures of methanol as

$$X = \frac{p_{\mathrm{MeOH},0} - p_{\mathrm{MeOH},t}}{p_{\mathrm{MeOH},0} + p_{\mathrm{MeOH},t}}. \tag{20}$$

Likewise, the contact time τ was determined by considering the increase in volume in the catalyst bed during

Table 2
Reaction orders for the components involved in the kinetic model

SRM		RWGS		MD	
Component	Reaction order	Component	Reaction order	Component	Reaction order
MeOH	0.6	CO_2	1.0	MeOH	1.3
H_2O	0.4	H_2	1.0		
CO_2	1.0	CO	1.0		
H_2	1.0	H_2O	1.0		

conversion. We calculated this by integrating the progress of conversion $X(\ell)$ as a function of the reactor length ℓ inside the catalyst bed

$$\tau = \frac{1}{\ell}\int_0^{\ell} \tau(\ell)\,\mathrm{d}\ell = \frac{A}{w_0}\int_0^{\ell} \frac{1}{1+X(\ell)}\,\mathrm{d}\ell, \tag{21}$$

where A is the cross section of the reactor and w_0 is the initial flow rate of the reactants. Furthermore, $X(\ell)$ may be sufficiently well approximated by an exponential function,

$$X(\ell) = 1 - \mathrm{e}^{-\omega\ell}, \tag{22}$$

and the parameter ω can be obtained from the values of the final conversion X_f and the final length of the catalyst bed ℓ_f

$$\omega = -\frac{\ln(1-X_\mathrm{f})}{\ell_\mathrm{f}}. \tag{23}$$

The kinetic evaluation was performed with the Berkeley Madonna 8.0.1 software. A Runge-Kutta method was used to solve the differential equations [Eqs. (15)–(19)], and the experimental data were fitted by a least-squares method. We determined the rate constants for the model reactions by fitting the simulation to the experimental data by varying the reaction orders until a good agreement was obtained, and this procedure was repeated until an optimal fit was achieved. According to the previous results of Purnama et al., the total reaction order for SRM ($m_1 + m_2$) was 1, whereas the individual reaction orders determined experimentally for methanol and water were 0.6 and 0.4, respectively [21]. The application of the above reaction orders ensured an optimal fit for the current experimental data. For the components involved in the RWGS reaction, the reaction orders were set to 1 [21], in correlation with those published by Choi and Stenger in their detailed study on the kinetics of the WGS reaction [48], including rate expressions derived from various reaction mechanisms [49]. The rate constants for both the RWGS and the MD reactions were considerably smaller than that of SRM, as revealed by the low CO production, and thus the reaction orders of the components implied in RWGS and MD had no appreciable effect on the fitting results. The reaction orders are summarized in Table 2.

The partial pressures for the components of the product stream were determined as a function of the contact time at temperatures of 503, 523, 543, and 573 K for all catalysts. The results obtained for CZC15 are displayed in Figs. 7–10. No significant differences were observed between the respective data for the other CZC samples.

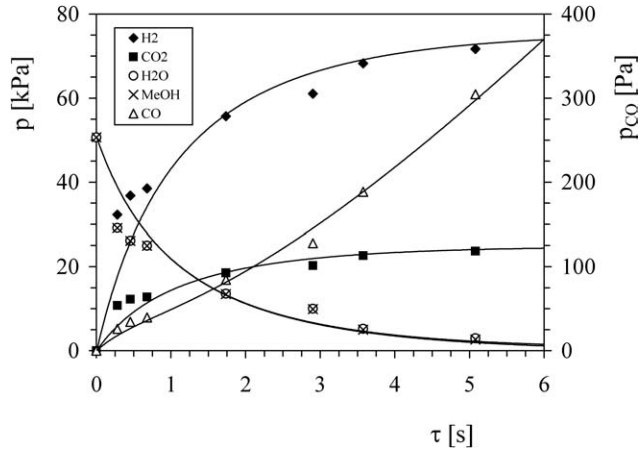

Fig. 7. Partial pressures of the components in the reaction mixture during SRM on CZC15; experimental data and fitting results: $m = 0.6726$ g, $T = 503$ K, $p = 10^5$ Pa, MeOH/H_2O = 1/1.

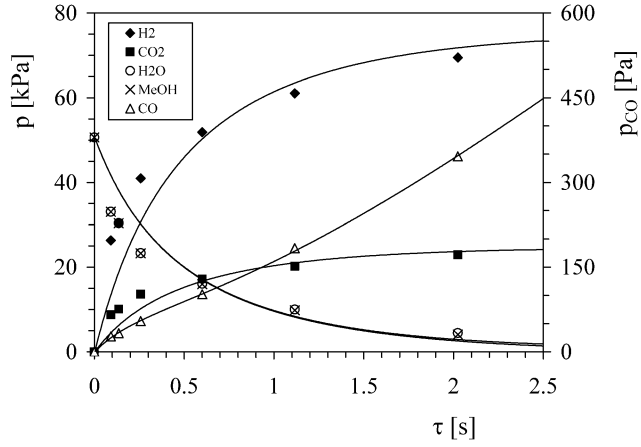

Fig. 8. Partial pressures of the components in the reaction mixture during SRM on CZC15; experimental data and fitting results: $m = 0.6726$ g, $T = 523$ K, $p = 10^5$ Pa, MeOH/H_2O = 1/1.

It can be seen from Figs. 7–10 that the partial pressures of the reactants methanol and water decreased to the same extent with increasing contact times at all temperatures. The most pronounced decrease can be observed at 573 K, where complete transformation occurred at $\tau < 1$ s. Meanwhile, the partial pressures of the main reaction products H_2 and CO_2 increased steadily during reaction and could be fitted with saturation curves, for which the limits for H_2 and CO_2 production proved to be 70–75 and 24 kPa, respectively. This implies that the amount of H_2 gained in the reaction at 573 K

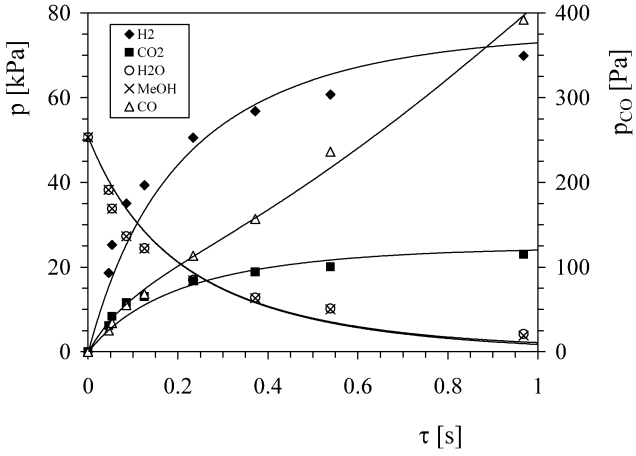

Fig. 9. Partial pressures of the components in the reaction mixture during SRM on CZC15, experimental data and fitting results: $m = 0.6726$ g, $T = 543$ K, $p = 10^5$ Pa, $MeOH/H_2O = 1/1$.

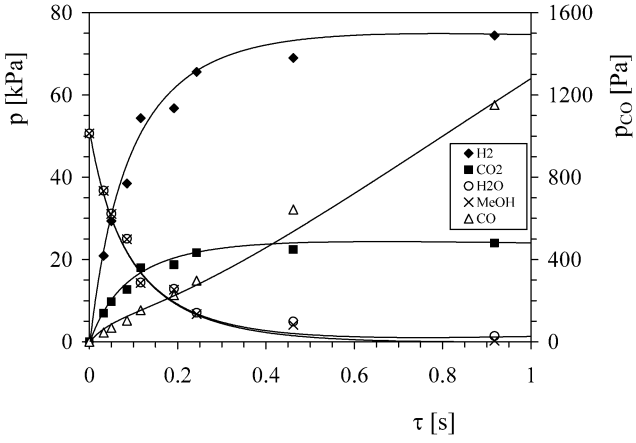

Fig. 10. Partial pressures of the components in the reaction mixture during SRM on CZC15; experimental data and fitting results: $m = 0.6726$ g, $T = 573$ K, $p = 10^5$ Pa, $MeOH/H_2O = 1/1$.

attains the theoretical maximum of 75%, corresponding to the thermodynamic equilibrium state [4], and approaches it reasonably well at lower temperatures. The differences in the partial pressures of H_2 and CO_2 at various contact times confirm that the amount of H_2 formed in the reaction was 3 times higher than that of CO_2, irrespective of the reaction temperature and the conversion level. With increasing contact time, CO_2 formation was less affected than H_2 production, and the contact time required to reach the saturation value decreased with the reaction temperature to an appreciable extent.

Compared with a commercial $Cu/ZnO/Al_2O_3$ catalyst [21], the H_2 partial pressures obtained for the CZC samples were somewhat lower (74–85% of those reported for the commercial sample between 503 and 573 K, respectively) at short contact times. Nevertheless, the saturation values observed for the CZC catalysts at long contact times approached 75 kPa at all temperatures.

The minor amount of CO detected in the reaction mixture was found to increase with both the contact time and the reaction temperature. In the temperature range investi-

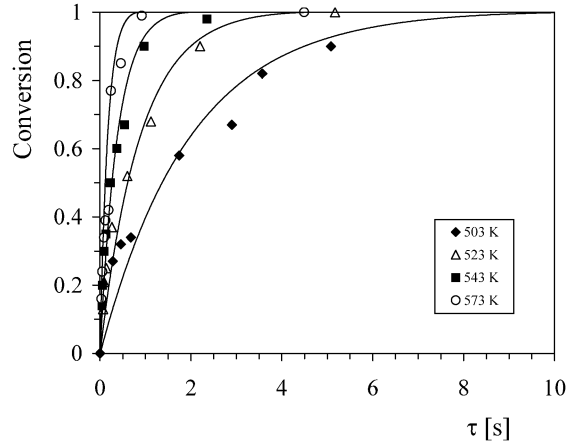

Fig. 11. Methanol conversions during SRM of CZC15 as a function of contact time at different reaction temperatures ($m = 0.6726$ g, $p = 10^5$ Pa, $MeOH/H_2O = 1/1$).

gated, the amount of CO typically varied between 0.06% and 0.4%, only exceeding that at 573 K, at contact times longer than 0.4 s. Unlike the main reaction products, the formation of CO can be described with S-shaped curves at each temperature, which may be regarded as further evidence that CO is a secondary product in the reaction [6,21]. As shown in Figs. 7–10, the partial pressures of CO could be fitted at all temperatures and contact times when MD was included in the reaction scheme. Nevertheless, it should be noted that the significance of MD can be observed only at low contact times, and therefore CO production is suggested to occur predominantly by the RWGS reaction. The conversions obtained for CZC15 at different temperatures, plotted as a function of the contact time, are displayed in Fig. 11.

The complete transformation of methanol could be achieved at all reaction temperatures, except for 503 K, where the contact time corresponding to full conversion was determined by extrapolation ($\tau \sim 10$ s). It can be seen that an increase in the reaction temperature resulted in a marked decrease in the contact time corresponding to the same conversion level. Accordingly, the full conversion of methanol at 573 K was observed at a contact time of 0.92 s. Although an increase in the reaction temperature proved to be beneficial in terms of the catalytic activity, as suggested by Fig. 11, it also resulted in the formation of an increased amount of CO in the product mixture (see Fig. 12). Furthermore, a prolonged exposure of the catalyst to 573 K was found to result in a moderate deactivation, which may be due to sintering of the active Cu particles [6,47]. For the other CZC samples, similar observations have been made. Likewise, Lindström and Pettersson reported that sintering of Cu particles of a $Cu/ZnO/Al_2O_3$ catalyst subjected to 613 K resulted in a loss of Cu surface area [50]. Hence, the optimal reaction temperature range for the steam reforming of methanol on CZC catalysts is 523–543 K, at which high methanol conversions can be achieved while a low CO level is maintained.

For the CO partial pressures, we fitted the experimental data by setting the final values, calculated at long contact

Table 3
Reaction rate constants determined for the SRM, RWGS and MD reactions on the CZC catalysts at different reaction temperatures

Sample	k_R[a,d] ($s^{-1}\,g^{-1}$)				k_{-W}[b,d] ($bar^{-1}\,s^{-1}\,g^{-1}$)				k_D[c,d] ($bar^{-0.3}\,s^{-1}\,g^{-1}$)			
	503 K	523 K	543 K	573 K	503 K	523 K	543 K	573 K	503 K	523 K	543 K	573 K
CZC5	2.92	10.71	34.40	68.44	0.04	0.11	0.30	1.12	0.04	0.13	0.66	2.12
CZC15	22.58	50.67	117.33	268.02	0.27	0.60	1.28	3.55	0.09	0.36	1.02	2.89
CZC25	20.25	55.17	79.95	146.37	0.22	0.95	1.35	3.06	0.14	0.38	1.13	4.50
CZC35	26.67	61.33	89.00	165.69	0.31	0.58	1.54	2.31	0.36	0.96	1.54	3.44

[a] Reaction rate constant of SRM.
[b] Reaction rate constant of RWGS.
[c] Reaction rate constant of MD.
[d] All values were referred to a CuO content of 1.0 g.

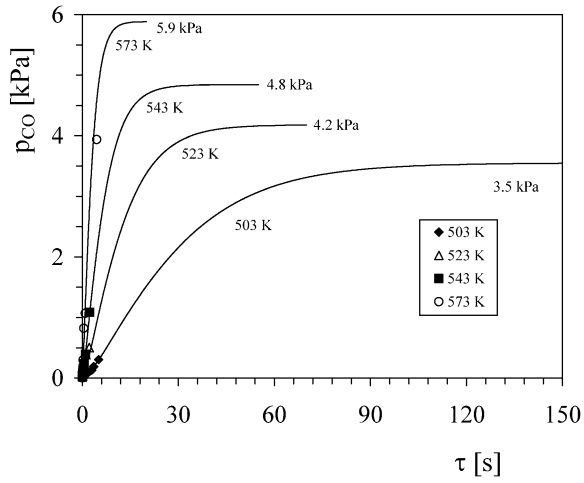

Fig. 12. CO partial pressures during SRM of CZC15 as a function of contact time at different reaction temperatures ($m = 0.6726$ g, $p = 10^5$ Pa, $MeOH/H_2O = 1/1$).

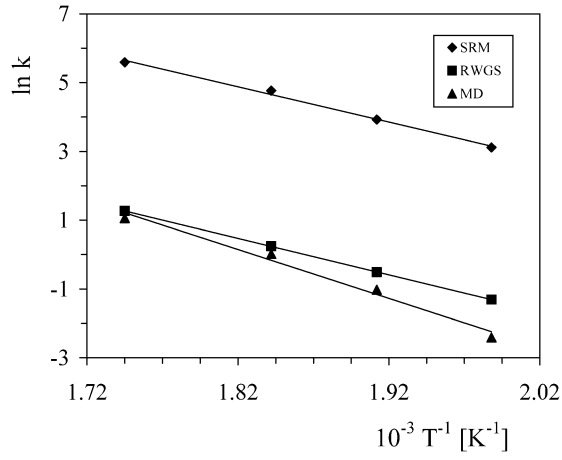

Fig. 13. Arrhenius plots for the SRM, RWGS and MD reactions determined for CZC15.

times from the thermodynamical equilibrium constant of the RWGS reaction, as displayed in Fig. 12. For comparison, we also determined these values experimentally by investigating a large amount of catalyst ($m = 3.55$ g) at a low flow rate of 0.01 $cm^3\,min^{-1}$ to ensure an extended contact time for the reaction. The CO partial pressures obtained from repeated runs at different temperatures were in good agreement with the theoretical values. It can be observed in Fig. 12 that the experimental CO levels are located at the low end of the theoretical curves and, hence, are far below those predicted by equilibrium calculations at all temperatures. It follows that the limiting CO partial pressures could be attained only at contact times considerably longer than those obtained under the present experimental conditions (see also Figs. 7–10). Accordingly, it is reasonable to assume that the kinetics of the CO formation is more complex than that described within the framework of this study [21]. Nevertheless, the kinetic model employed provides a good approximation for the experimental data obtained for all components in the contact time region where complete methanol conversion occurs, which may be of major interest for industrial applications.

The reaction rate constants (k) for the individual reactions, obtained from the simulations performed by application of the reaction orders indicated in Table 2, are listed in Table 3. For a better comparison, all values were referred to a CuO content of 1.0 g.

For the most active catalyst (CZC35) investigated at the highest reaction temperature (573 K), the Thiele modulus [51] was calculated to be 0.594, from which the mass transfer factor (the actual reaction rate as referred to the ideal reaction rate without transport limitation) was 0.977, indicating that the mass transport limitation was indeed negligible and thus the reaction was kinetically controlled. Given that the reaction rates for the other CZC samples were found to be typically lower, in particular at temperatures below 573 K, the effect of intraparticle transport phenomena on the kinetic parameters can be safely excluded.

The apparent activation energies were determined from the slopes of the Arrhenius plots

$$\ln(k) = \ln(k_0) - \frac{E_A}{RT}. \tag{24}$$

A typical illustration of the Arrhenius parameters for the model reactions on CZC15 is displayed in Fig. 13. It may readily be observed from the slopes that the activation energies of SRM and RWGS are comparable and considerably lower than that of MD. The values of the activation energies for the SRM, RWGS, and MD reactions, determined for all of the CZC samples, are listed in Table 4.

Table 4
Apparent activation energies for the SRM, RWGS and MD reactions on the CZC catalysts

Reaction	E_A (kJ mol^{-1}) CZC5	E_A (kJ mol^{-1}) CZC15	E_A (kJ mol^{-1}) CZC25	E_A (kJ mol^{-1}) CZC35
SRM	109.2	85.4	66.1	60.7
RWGS	115.5	88.2	85.7	69.3
MD	142.6	118.7	104.9	75.5

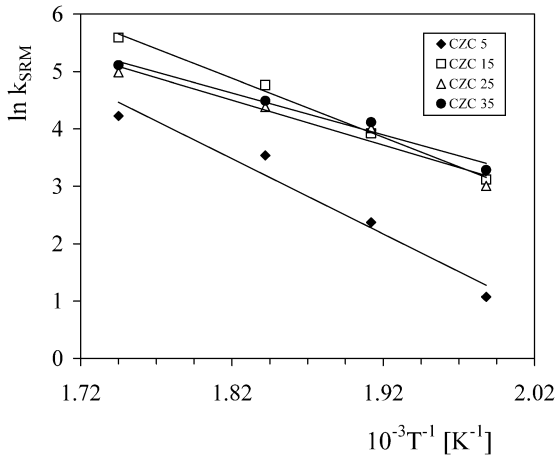

Fig. 14. Arrhenius representation of the reaction rate constants obtained for the SRM reaction on the CZC catalysts.

According to Table 4, no significant differences between the activation energies of the SRM and RWGS reactions can be observed, except for CZC25. For the latter sample, the activation energy of the RWGS reaction was considerably higher than that for SRM, which may account for the particularly low CO level observed for this catalyst (see Fig. 4). On the other hand, the activation energies for MD proved to be considerably higher than those for SRM and RWGS, and therefore MD may be regarded as the rate-limiting step for CO formation at short contact times. As mentioned above, the significance of MD in the overall reaction mechanism decreases dramatically at contact times exceeding 0.3–1 s, depending on the reaction temperature. Accordingly, the enhanced CO levels obtained at longer contact times can be attributed to the predominance of the RWGS reaction, which requires a considerably lower activation energy.

For the main reaction (SRM), the apparent activation energies proved to be relatively close for all samples, apart from CZC5, for which the highest value was obtained. For comparison, the Arrhenius plots for all of the CZC samples are depicted in Fig. 14. For CZC5 and CZC15, the apparent activation energies are in good agreement with those reported in the literature for Cu/ZnO/Al_2O_3 catalysts, whereas the values for CZC25 and CZC35 are lower [6,16,21,52].

For all of the model reactions (SRM, RWGS, and MD), the activation energies determined exhibit a linear correlation with the Cu content, as shown in Fig. 15. With an increasing amount of Cu, a systematic decrease was found for each reaction. The most pronounced decrease can be observed in the activation energy of MD, indicating that at lower Cu loading the contribution of MD to CO formation diminishes. Takeguchi et al. have reported a similar trend for the SRM reaction on two Cu/ZnO catalysts [53], although a potential mass transport limitation was not taken into account, and thus their studies cannot be directly compared with the results presented here. Conversely, in the current study, the well-known effect of mass transport limitation on the kinetic studies, resulting in a reduced apparent activation energy, can be excluded. Therefore, it is concluded that the variation of the Cu concentration in the CeO_2/ZrO_2 precursor material gave rise to the formation of CZC samples with significantly different catalytic behavior. Whereas the chemical complexity in the various CZC catalysts remains the same, the chemical composition adjusted in the preparation procedure results in a significantly altered structural complexity of the materials. These catalysts with vastly different active surfaces exhibit a catalytic behavior that is not simply correlated with the accessible surface area. Dispersion, Cu particle size, and Cu support interactions have a pronounced influence on the microstructure of the Cu particles and the effect of the microstructure on the active Cu surface. Eventually, researchers must elucidate both the Cu surface area and the microstructural properties of the Cu particles to fully understand the significantly different catalytic activities and the kinetics described above.

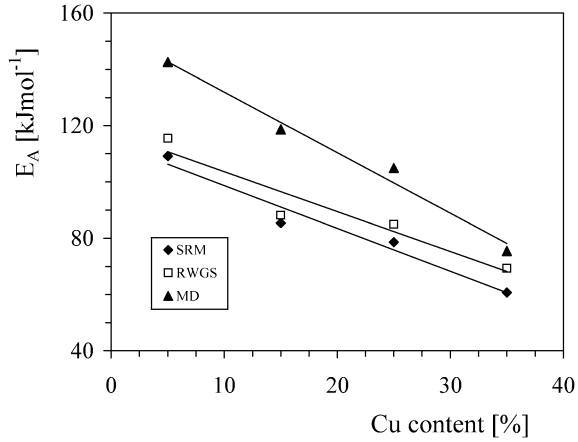

Fig. 15. Apparent activation energies of the model reactions (SRM, RWGS, and MD) as a function of the Cu content of four CZC catalysts.

4. Conclusions

Novel Cu/ZrO_2/CeO_2 materials prepared by coprecipitation and polymer templating were investigated as catalysts in the steam reforming of methanol. Catalytic measurements were performed under continuous operation in a fixed-bed reactor at atmospheric pressure. Time-on-stream experiments indicated that after an initial period of deactivation, the conversions for the samples with Cu contents exceeding 5% were stabilized, and thus these samples could be suitable for prolonged catalytic applications. An increase

in the Cu content from 5 to 15% was found to improve the long-term stability and suppress the CO production considerably, whereas the effect of a further enhancement was less significant. With respect to a reduced formation of CO during SRM, the samples with increased Cu loading proved to be more efficient catalysts.

Since the effect of mass transport limitations on the catalytic reaction was found to be insignificant, a kinetic analysis was undertaken. The reaction scheme suggested for the overall transformation included the SRM, MD, and RWGS reactions. The experimental data obtained in the range of 503–573 K could be well fitted by the kinetic model employed. The optimal temperature range for SRM on the CZC catalysts was 523–543 K, for which high methanol conversions and low CO levels were obtained. For the SRM and RWGS reactions, the values of the activation energies were comparable and considerably lower than that of MD. The activation energy of each reaction exhibited a systematic decrease with increasing Cu content of the catalyst. Evidently, the variation in the Cu concentration of the precursor material during preparation altered the microstructure of the Cu particles and, thus, the active Cu surface, which considerably affected the catalytic behavior of the CZC catalysts.

References

[1] B. Lindström, L.J. Pettersson, Int. J. Hydrogen Energy 26 (2001) 923.
[2] S. Velu, K. Suzuki, M. Okazaki, M.P. Kapoor, T. Osaki, F. Ohashi, J. Catal. 194 (2000) 373.
[3] J.P. Breen, J.R.H. Ross, Catal. Today 51 (1999) 521.
[4] P.J. de Wild, M.J.F.M. Verhaak, Catal. Today 60 (2000) 3.
[5] J. Agrell, H. Birgersson, M. Boutonnet, I. Melian-Cabrera, R.M. Navarro, J.L.G. Fierro, J. Catal. 219 (2003) 389.
[6] J. Agrell, H. Birgersson, M. Boutonnet, J. Power Sources 4654 (2002) 1.
[7] G.A. Olah, Catal. Lett. 93 (2004) 1.
[8] B. Lindström, L.J. Pettersson, J. Power Sources 106 (2002) 264.
[9] J. Agrell, M. Boutonnet, J.L.G. Fierro, Appl. Catal. A 253 (2003) 213.
[10] S. Velu, K. Suzuki, T. Osaki, Chem. Commun. (1999) 2341.
[11] J. Papavasiliou, G. Avgouropoulos, T. Ioannides, Catal. Commun. 5 (2004) 231.
[12] X.R. Zhang, P. Shi, J. Zhao, M. Zhao, C. Liu, Fuel Proces. Technol. 83 (2003) 183.
[13] K. Takahashi, N. Takezawa, H. Kobayashi, Appl. Catal. 2 (1982) 383.
[14] E. Santacesaria, S. Carra, Appl. Catal. 5 (1983) 345.
[15] J.C. Amphlett, R.F. Mann, R.D. Weir, Can. J. Chem. Eng. 66 (1988) 950.
[16] C.J. Jiang, D.L. Trimm, M.S. Wainwright, Appl. Catal. A 93 (1993) 245.
[17] N. Iwasa, S. Masuda, N. Ogawa, N. Takezawa, Appl. Catal. A 125 (1995) 145.
[18] C. Cao, G. Xia, J. Holladay, E. Jones, Y. Wang, Appl. Catal. A 262 (2004) 19.
[19] W.H. Cheng, I. Chen, J. Liou, S.S. Lin, Top. Catal. 22 (2003) 225.
[20] M.V. Twigg, M.S. Spencer, Top. Catal. 22 (2003) 191.
[21] H. Purnama, T. Ressler, R.E. Jentoft, H. Soerijanto, R. Schlögl, R. Schomäcker, Appl. Catal. A 259 (2004) 83.
[22] M.M. Günter, T. Ressler, R.E. Jentoft, B. Bems, J. Catal. 203 (2001) 133.
[23] B.L. Kniep, T. Ressler, A. Rabis, F. Girgsdies, M. Baenitz, F. Steglich, R. Schlögl, Angew. Chem. Int. Ed. 43 (2004) 112.
[24] T. Shishido, Y. Yamamoto, H. Morioka, K. Takaki, K. Takehira, Appl. Catal. A 263 (2004) 249.
[25] B.A. Peppley, J.C. Amphlett, L.M. Kearns, R.F. Mann, Appl. Catal. A 179 (1999) 21.
[26] S.P. Asprey, B.W. Wojciechowski, B.A. Peppley, Appl. Catal. A 179 (1999) 51.
[27] H. Purnama, F. Girgsdies, T. Ressler, J.H. Schattka, R.A. Caruso, R. Schomäcker, R. Schlögl, Catal. Lett. 94 (2004) 61.
[28] J.P. Breen, F.C. Meunier, R.H. Ross, Chem. Commun. (1999) 2247.
[29] P.H. Matter, D.J. Braden, U.S. Ozkan, J. Catal. 223 (340) (2004).
[30] X. Zhang, P. Shi, J. Mol. Catal. A 194 (2003) 99.
[31] Y. Liu, T. Hayakawa, K. Suzuki, S. Hamakawa, T. Tsunoda, T. Ishii, M. Kumagai, Appl. Catal. A 223 (2002) 137.
[32] H.S. Roh, K.W. Jun, W.S. Dong, S.E. Park, Y.S. Baek, Catal. Lett. 74 (2001) 31.
[33] M.F. Luo, J. Chen, L.S. Chen, J.Q. Lu, Z. Feng, C. Li, Chem. Mater. 13 (2001) 197.
[34] B.C. Gates, Catalytic Chemistry, Wiley, New York, 1992.
[35] A.S. Deshpande, N. Pinna, P. Beato, M. Antonietti, M. Niederberger, Chem. Mater. 16 (2004) 2599.
[36] G.C. Chinchen, C.M. Hay, H.D. Vandervell, K.C. Waugh, J. Catal. 103 (1987) 79.
[37] M.M. Günter, T. Ressler, B. Bems, C. Büscher, T. Genger, O. Hinrichsen, M. Muhler, R. Schlögl, Catal. Lett. 71 (2001) 37.
[38] R.A. Young, The Rietveld Method, Oxford University Press, New York, 1993.
[39] Y. Choi, H.G. Stenger, Appl. Catal. B 38 (2002) 259.
[40] J. Agrell, M. Boutonnet, I. Melian-Cabrera, J.L.G. Fierro, Appl. Catal. A 253 (2003) 201.
[41] E.D. Schrum, T.L. Reitz, H.H. Kung, Stud. Surf. Sci. Catal. 139 (2001) 229.
[42] J.C. Amphlett, M.J. Evans, R.F. Mann, R.D. Weir, Can. J. Chem. Eng. 63 (1985) 605.
[43] J.C. Amphlett, R.F. Mann, B.A. Peppley, Stud. Surf. Sci. Catal. 81 (1994) 409.
[44] H. Kobayashi, N. Takezawa, C. Minochi, Chem. Lett. (1976) 1347.
[45] K. Takahashi, N. Takezawa, H. Kobayashi, Appl. Catal. 2 (1982) 383.
[46] M.S. Spencer, Nature 323 (1986) 685.
[47] M.V. Twigg, M.S. Spencer, Appl. Catal. A 212 (2001) 161.
[48] Y. Choi, H.G. Stenger, J. Power Sources 124 (2003) 432.
[49] N. Amadeo, M. Laborde, Int. J. Hydrogen Energy 20 (1995) 949.
[50] B. Lindström, L.J. Pettersson, Catal. Lett. 74 (2001) 27.
[51] O. Levenspiel, Chemical Reaction Engineering, Wiley, New York, 1972.
[52] K. Geissler, E. Newson, F. Vogel, T.B. Truong, P. Hottinger, A. Wokaun, Phys. Chem. Chem. Phys. 3 (2001) 47.
[53] T. Takeguchi, Y. Kani, M. Inoue, K. Eguchi, Catal. Lett. 83 (2002) 49.